The Astrophysical Journal Letters, 864:L35 (6pp), 2018 September 10
https://doi.org/10.3847/2041-8213/aadd46

Red versus Blue: Early Observations of Thermonuclear Supernovae Reveal Two Distinct Populations?

Maximilian D. Stritzinger[1,7], Benjamin J. Shappee[2], Anthony L. Piro[3], Christopher Ashall[4],
E. Baron[5,8], Peter Hoeflich[4], Simon Holmbo[1], Thomas W.-S. Holoien[3], M. M. Phillips[6], C. R. Burns[3],
Carlos Contreras[6], Nidia Morrell[6], and Michael A. Tucker[2]
[1] Department of Physics and Astronomy, Aarhus University, Ny Munkegade 120, DK-8000 Aarhus C, Denmark; max@phys.au.dk
[2] Institute for Astronomy, University of Hawai'i, 2680 Woodlawn Drive, Honolulu, HI 96822, USA
[3] The Observatories of the Carnegie Institution for Science, 813 Santa Barbara Street, Pasadena, CA 91101, USA
[4] Department of Physics, Florida State University, 77 Chieftain Way, Tallahassee, FL, 32306, USA
[5] Homer L. Dodge Department of Physics and Astronomy, University of Oklahoma, 440 West Brooks, Room 100, Norman, OK 73019-2061, USA
[6] Carnegie Observatories, Las Campanas Observatory, Casilla 601, La Serena, Chile

Received 2018 June 27; revised 2018 August 24; accepted 2018 August 28; published 2018 September 11

Abstract

We examine the early phase intrinsic $(B-V)_0$ color evolution of a dozen SNe Ia discovered within three days of the inferred time of first light ($t_{\rm first}$) and have $(B-V)_0$ color information beginning within five days of $t_{\rm first}$. The sample indicates there are two distinct early populations. The first is a population exhibiting blue colors that slowly evolve, and the second population exhibits red colors and evolves more rapidly. We find that the early blue events are all 1991T/1999aa-like with more luminous, slower declining light curves than those exhibiting early red colors. Placing the first sample on the Branch diagram (i.e., ratio of Si II λλ5972, 6355 pseudo-Equivalent widths) indicates that all blue objects are of the Branch shallow silicon (SS) spectral type, while all early red events except for the 2000cx-like SN 2012fr are of the Branch Core Normal (CN) or CooL (CL) type. A number of potential processes contributing to the early emission are explored, and we find that, in general, the viewing-angle dependance inherent in the companion collision model is inconsistent with all of the SS objects with early-time observations being blue and exhibiting an excess. We caution that great care must be taken when interpreting early phase light curves as there may be a variety of physical processes that are possibly at play and significant theoretical work remains to be done.

Key words: supernovae: general

1. Introduction

SNe Ia are well-studied astrophysical events generally thought to be the thermonuclear disruption of a carbon–oxygen (C/O) white dwarf (WD) in a binary system. In order for future SN Ia experiments to expand upon our knowledge of dark energy, a substantial improvement in their accuracy as distance indicators is required. This is likely only to be achieved by increasing our understanding of SNe Ia progenitors and their explosion physics. Early phase observations of SNe Ia offer a unique window to better understand their origins. To date early observations have allowed for a direct constraint on the size of the WD progenitor of SN 2011fe (Nugent et al. 2011; Bloom et al. 2012) using the lack of a shock cooling signal (Piro et al. 2010), and in about a dozen cases, have provided robust constraints on the size of any potential companion (Bloom et al. 2012; Foley et al. 2012; Silverman et al. 2012; Zheng et al. 2013; Goobar et al. 2015; Im et al. 2015; Olling et al. 2015; Marion et al. 2016; Shappee et al. 2016, 2018; Cartier et al. 2017; Hosseinzadeh et al. 2017; Miller et al. 2018).

To date nearly 20 SNe Ia have been discovered within three days of their inferred time of first light ($t_{\rm first}$),[9] and this sample exhibits interesting diversity. The early light curves of one group rise exponentially and are typically well fit by a single power-law function (e.g., Nugent et al. 2011; Olling et al. 2015). In a second group, the early light curves exhibit a ≈3 day linear rise in flux followed by an exponential rise (e.g., Hosseinzadeh et al. 2017; Contreras et al. 2018; Miller et al. 2018). Such objects are well fit with a double (or broken) power-law fit (e.g., Zheng et al. 2013, 2014). It is a matter of open debate as to what physics is driving single versus double power-law fit SN Ia ,with possibilities ranging from companion interaction (Kasen 2010; Maeda et al. 2014) to enhanced mixing of radioactive elements (Piro & Nakar 2013; Piro & Morozova 2016; Magee et al. 2018). Furthermore, the full diversity of early phase properties is likely far from fully explored. This point is highlighted by the early light curve of MUSSES1604. In this case the supernova exhibited an optical flash associated with a $m_g \approx 2$ mag increase in brightness within 24 hr of explosion, followed by a short 24 hr plateau period, and then subsequently, it continued to brighten similarly to other SNe Ia (Jiang et al. 2017).

In the following, we collect a sample of early phase SN Ia observations in order to examine their intrinsic $(B-V)_0$ color evolution. We then examine the location of the sample objects along the Phillips relation and the Branch et al. (2006) diagram. We find that SNe Ia exhibiting blue, slowly evolving $(B-V)_0$ colors are also of the Branch shallow silicon (SS) spectral type as compared to red, more rapidly evolving objects. This suggests at least two distinct populations of SNe Ia. The host properties of the sample are also examined and our findings are placed into context with leading models.

---

[7] Visiting Astronomer, Institute for Astronomy, University of Hawai'i, 2680 Woodlawn Drive, Honolulu, HI 96822, USA.

[8] Visiting Astronomer, Hamburger Sternwarte, Gojenbergsweg 112, D-21029 Hamburg, Germany.

[9] In this work we refer to $t_{\rm first}$ as the explosion epoch, however, it is possible that some SN Ia experience a 1–2 day dark phase between the explosion and $t_{\rm first}$ (Piro & Nakar 2013).

2. Data Sample

We have combed the literature to identify all objects useful to explore the diversity among the early color evolution of SNe Ia. Two selection criteria were imposed. First the discovery must have occurred within three days of $t_{\rm first}$, and second, each object has early B- and V-band light curves. We found 13 objects fulfilling these criteria and present them in Table 1, along with a number of pertinent details including: host designation and redshift, Milky Way and host-galaxy reddening, inferred $t_{\rm first}$, and $t_{\rm rise}$, and additionally, estimates of the light curve decline rate parameter $\Delta m_{15}(B)$[10], peak absolute B-band magnitude (M_B), Branch et al. (2006) and Wang et al. (2009) spectral types, our early color subtyping (i.e., red or blue; see Section 3.1), and references to adopted host-reddening values, data, and/or adopted values of $t_{\rm first}$.

We note that two members of the early sample—SN 2009ig and SN 2012fr—have been pointed out to be somewhat peculiar (Contreras et al. 2018) as they exhibit similarities to SN 2000cx (Li et al. 2001). These two objects are include in our early sample since both objects are fully consistent with the luminosity decline rate relation (see Foley et al. 2012; Contreras et al. 2018, and below) and their early light curve evolution is not peculiar as in the case of MUSSES1604D. MUSSES1604D itself is a 2006bt-like event (e.g., Foley et al. 2010; Stritzinger et al. 2011) with photometric and spectroscopic characteristics that differ significantly at early and maximum phase compared to the rest of our sample (Jiang et al. 2017). However, as it does fulfil our selection criteria, it is included in our sample for completeness as a green symbol in the figures presented below.

Figure 1 contains a color image of each host galaxy of the early sample with the location of the supernova indicated with a star (color coded red or blue; see below). According to the NASA/IPAC Extragalactic Database (NED), all members of our early sample are hosted in spiral galaxies, except the host of MUSSES1604D, which is an S0 galaxy (Jiang et al. 2017). No obvious trends are found between early color type and host properties and/or the locations of the supernovae relative to their hosts.

3. Results

3.1. Early Sample $(B-V)_0$ Color Evolution

Figure 2 contains the intrinsic $(B-V)_0$ color evolution for the early sample, color coded in either red or blue. The color curves have been corrected for both Milky Way reddening, host-galaxy reddening and time dilation. Red objects exhibit $(B-V)_0 \gtrsim 0.2$ mag by $+2$ days, and as much as ≈ 0.5 mag at $+0.5$ days. The color of the blue objects ranges between $(B-V)_0 \sim -0.2$ to 0.05 mag within the first $+2$ days relative to $t_{\rm first}$ and evolve relatively slowly compared to the red objects. By $+4$ days the color difference between the two groups is negligible.

Inspection of the color difference between the two populations reveal differences on the order of ~ 0.5 mag, which corresponds to a difference in flux of $\sim 50\%$. This is far too large of a flux difference to be attributed to spectral line features. Due to a scarcity of data, here we focus exclusively on $(B-V)_0$, however, we note that the blue versus red subtypes hold over different color combinations (see, e.g., Hosseinzadeh et al. 2017).

3.2. Early Sample on the M_B versus $\Delta m_{15}(B)$ Relation

Plotted in Figure 3 are the M_B and $\Delta m_{15}(B)$ values listed in Table 1 of the early sample along with a sample of 1991T-like, normal, and 1991bg-like supernovae observed by the Carnegie Supernova Project I (Krisciunas et al. 2017). Objects exhibiting early blue colors tend to exhibit higher peak luminosities and slower decline rates. Interestingly, the two red objects that are as bright as the majority of the early blue objects are both of the 2000cx-like objects (Contreras et al. 2018).

3.3. Early Sample on the Branch Diagram

We now examine the ratio of the pseudo-equivalent widths (pEWs) measured for the Si II $\lambda 5972$ and Si II $\lambda 6355$ spectral features in optical spectra obtained within three days of B-band maximum. This ratio is known to correlate with photospheric temperature (Nugent et al. 1995) and serves as basis for the Branch et al. (2006) spectral classifications consisting of: Core Normal (CN), Broad Lined (BL), shallow silicon (SS), and CooL (CL). CN are normal SN Ia. BL show higher than normal Si II $\lambda 6355$ Doppler velocity. Among the BL objects, two-thirds correspond to high-velocity (HV) objects in the Wang et al. (2009) classification scheme, as defined by exhibiting Si II $\lambda 6355$ Doppler velocity of $\geqslant 10{,}800$ km s^{-1} at maximum light. Finally, SS are typically bright 1991T/1999aa-like objects and the CL subtype contains both transitional and 1991bg-like SN Ia.

Figure 4 contains the Branch diagram populated with an extended sample of SNe Ia (Blondin et al. 2012), along with our early sample color coded red versus blue. Interestingly, aside from the peculiar 2000cx-like SN 2012fr (Contreras et al. 2018), all of the red objects are of the CN or CL subtype, and all of the blue objects are located in a relatively narrow region extending from SS to the interface with the edge of the CN population.

Although SN 2012fr follows the luminosity decline rate relation (see Figure 3), it is spectroscopically peculiar. At maximum light its Si II $\lambda 6355$ Doppler velocity is 12,000 km s^{-1} (Childress et al. 2013). This places SN 2012fr as a HV object in the Wang et al. system, while its Si II velocity remains essentially flat for a month past maximum (Childress et al. 2013). Following Benetti et al. (2005), SN 2012fr is a low-velocity gradient (LVG; i.e., velocity gradient $\dot{v} < 70$ km s^{-1} day^{-1}) object. Only $\approx 10\%$ of SNe Ia are found to be HV and LVG, while only $\approx 5\%$ of SNe Ia are also HV and SS+CN (see Contreras et al. 2018). Altogether with its peculiar spectroscopic attributes, we note one should approach SN 2012fr with caution when comparing its spectral diagnostics to our limited early sample.

4. Discussion

Using the early phase light curve colors, we have identified at least two distinct populations of SNe Ia, the properties of which are as follows.

1. Events that are blue at early times have spectra similar to 1991T/1999aa-like objects, fall within the Branch SS spectral type, and are typically more luminous at peak with a smaller $\Delta m_{15}(B)$.

---

[10] This parameter is the difference in magnitude between B-band peak and 15 days later and is known to correlate with M_B (Philips 1993).

Table 1
Early Color Evolution Sample Parameters

SN	Host	Redshift	$E(B-V)_{\rm MW}$ (mag)	$E(B-V)_{\rm host}$ (mag)	$t_{\rm first}$ (MJD)	$t_{\rm rise}$ (days)	$\Delta m_{15}(B)$ (mag)	M_B (mag)	Spectral Type[a]	Color	References(s)
2009ig	NGC 1015	0.00877	0.032	⋯	55062.9	17.1	0.90 ± 0.07	−19.46 ± 0.12	CN, HV	red	(1)
2011fe	M101	0.00080	0.008	⋯	55796.7	17.8	1.07 ± 0.06	−19.10 ± 0.19	CN, normal	red	(2)
2012cg	NGC 4424	0.00146	0.018	0.18 ± 0.05[b]	56061.8	19.5	0.86 ± 0.02	−19.62 ± 0.31	SS, 91T/99aa-like	blue	(3)
2012fr	NGC 1365	0.00546	0.018	0.03 ± 0.04[c]	56225.8	16.9	0.82 ± 0.03	−19.43 ± 0.14	CN+SS, HV	red	(4)
2012ht	NGC 3447	0.00356	0.025	0.05 ± 0.01[c]	56278.0	17.6	1.27 ± 0.05	−18.98 ± 0.07	CN, normal	red	(5)
2013dy	NGC 7250	0.00389	0.140	0.21 ± 0.01[d]	56483.4	17.7	0.92 ± 0.03	−19.65 ± 0.04	SS, 91T/99aa-like	blue	(6)
2013gy	NGC 1418	0.01402	0.049	0.11 ± 0.06[c]	56629.4	19.1	1.23 ± 0.06	−19.32 ± 0.16	CN, normal	red	(7)
iPTF 13ebh	NGC 890	0.01327	0.067	0.07 ± 0.02[c]	56607.9	14.8	1.76 ± 0.02	−18.95 ± 0.19	CL, normal	red	(8)
ASASSN-14lp	NGC 4666	0.00510	0.021	0.35 ± 0.01[c]	56998.5	16.7	0.80 ± 0.05	−19.36 ± 0.60	SS, 91T-like	blue	(9)
2015F	NGC 2442	0.00489	0.175	0.16 ± 0.03[c]	57088.4	18.5	1.25 ± 0.05	−19.47 ± 0.27	CN, normal	red	(10)
iPTF16abc	NGC 5221	0.02328	0.028	0.05 ± 0.03[e]	57481.6	17.9	0.85 ± 0.05	−19.20 ± 0.40	SS, normal/91T-like	blue	(11)
MUSSES1604D	⋯	0.11737	0.026	⋯	57481.8	22.4	1.00 ± 0.07	−18.80 ± 0.40	BL, HV	red	(12)
2017cbv	NGC 5643	0.00400	0.150	⋯	57821.9	18.3	1.06 ± 0.05	−20.04 ± 0.60	SS, 91T-like	blue	(13)

Notes.

[a] Branch et al. (2006) and Wang et al. (2009) spectral classifications.

[b] Silverman et al. (2012).

[c] Based on SNooPy fits to photometry obtained by the Carnegie Supernova Project-II (C. R. Burns et al. 2018, in preparation).

[d] Pan et al. (2015).

[e] Miller et al. (2018).

References. (1) Blondin et al. (2012), Foley et al. (2012), Marion et al. (2013), (2) Nugent et al. (2011), Vinkó et al. (2012), Pereira et al. (2013), (3) Silverman et al. (2012), Marion et al. (2016), (4) Contreras et al. (2018), (5) Yamanaka et al. (2012), This work; (6) Zheng et al. (2013), Pan et al. (2015), Zhai et al. (2016), (7) Holmbo et al. (2018), (8) Hsiao et al. (2015), (9) Shappee et al. (2016), this work; (10) Cartier et al. (2017), this work; (11) Miller et al. (2018), this work; (12) (Jiang et al. 2017), this work; (13) Hosseinzadeh et al. (2017), this work.

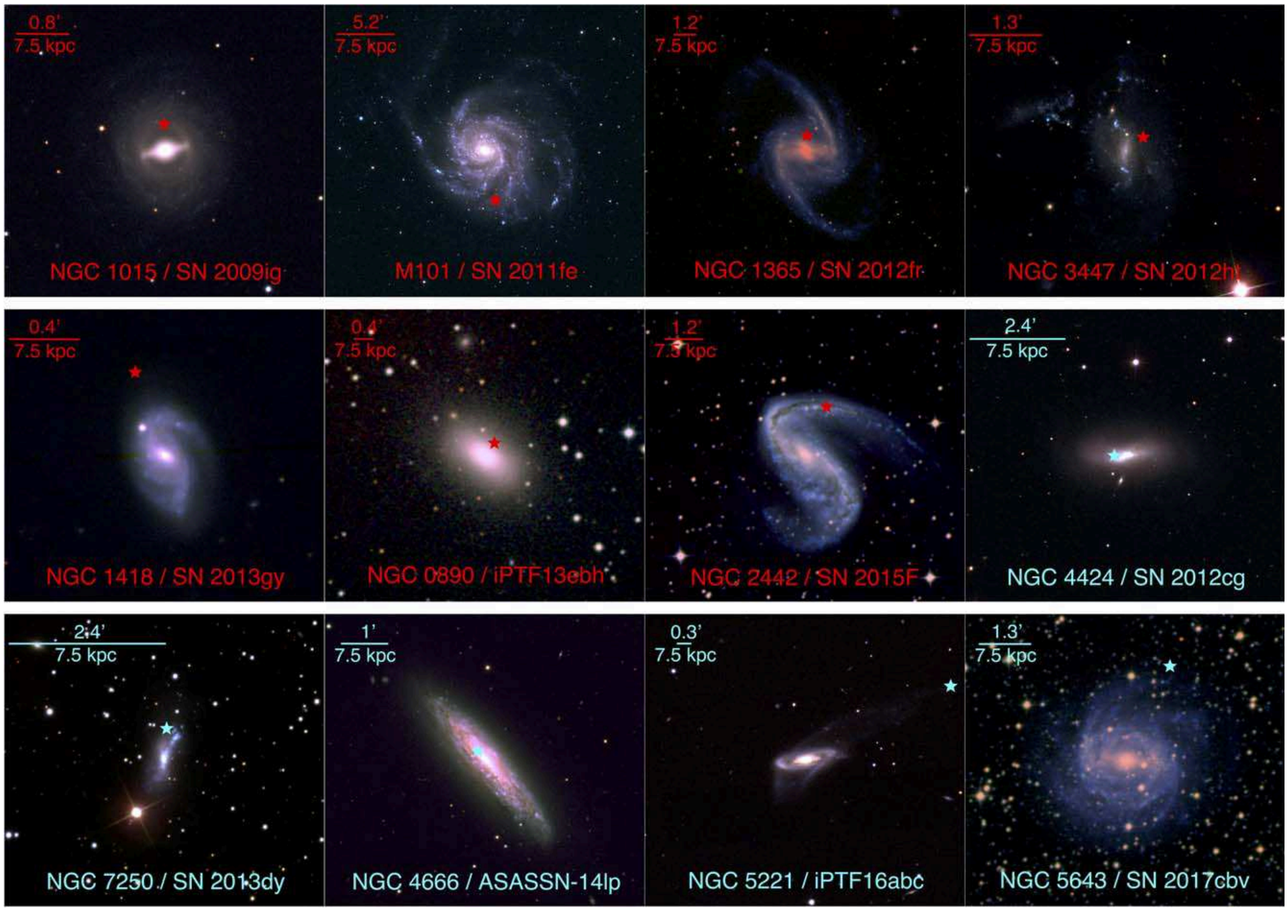

Figure 1. Mosaic of colored images of our early red vs. blue sample with the position of the SNe indicated with stars. Images were constructed using either the Sloan Digital Sky Survey *gri*-band, DSS IR-red-blue, or (in one case) Pan-STARRS *gri*-band archival images.

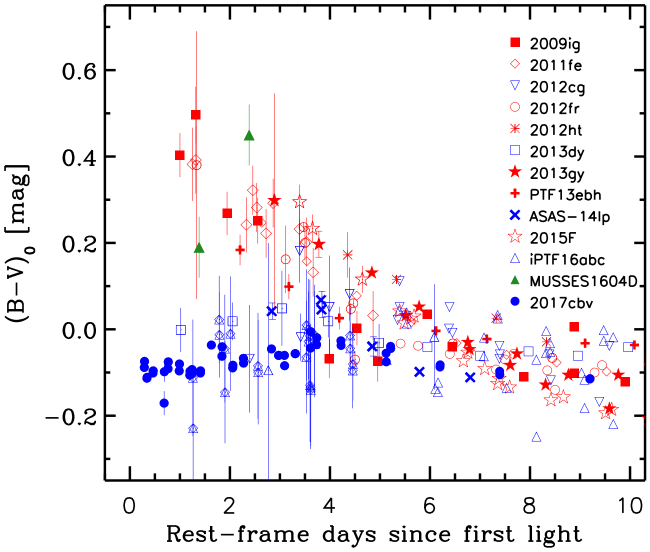

Figure 2. Optical $(B-V)_0$ color evolution for SNe Ia discovered within 3 days of first light, t_{first}. For presentation purposes error bars are included for all colors obtained within 5 days of t_{first}. The early evolution of the current sample indicates SNe Ia exhibit either red colors that rapidly evolve to the blue, or blue colors that evolve relatively slow over time. Time-dilation and reddening corrections have been applied using redshift and extinction values listed in Table 1.

2. Events that are red at early times are mostly of the Branch CN or CL spectral types (with the exception of one 2000cx-like object) and may typically be less luminous at peak with a larger $\Delta m_{15}(B)$.

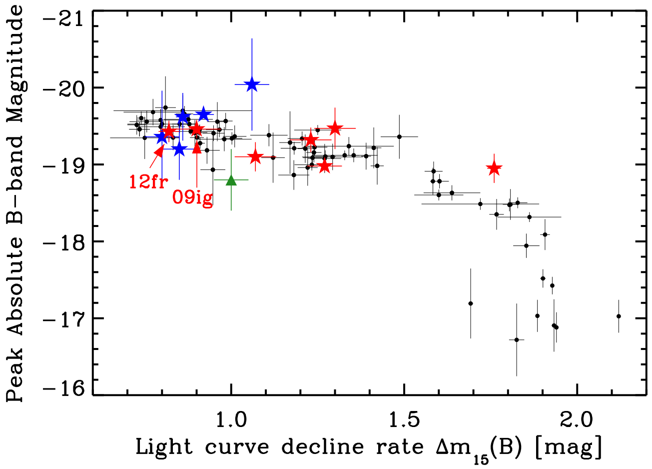

Figure 3. Luminosity decline rate relation consisting of 1991T-like, normal, and 1991bg-like SNe Ia observed by the Carnegie Supernova Project I (Krisciunas et al. 2017). Color stars correspond to the comparison sample with blue stars corresponding to objects with blue colors at early phases and red stars are those exhibiting red colors. Excluding the peculiar 2000cx-like SNe 2009ig and 2012fr, objects with early, slowly evolving blue colors are generally brighter and exhibit slower declining light curves than objects with early, rapidly evolving red colors.

We now briefly discuss various processes that may be contributing to the early phase emission. These range from interaction with a non-degenerate companion, the presence of HV ^{56}Ni, interaction with circumstellar material (CSM), and opacity differences in the outer layers of the ejecta.

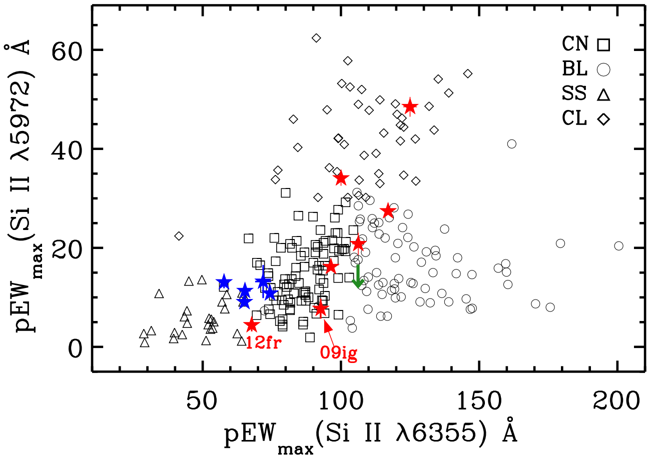

Figure 4. Branch diagram of the pEW values measured from the Si II λ5972 and Si II λ6355 absorption features in near maximum light spectra from the Blondin et al. (2012) sample along with pEW values measured of our early sample. The four Branch spectral types are indicated with different black symbols and the early sample is plotted as colored stars. All normal SNe Ia exhibiting blue colors are either of the SS subtype or lie just along the interface between the SS and CN types. Note that the λ5972 pEW measurement for MUSSES1604D is an upper limit.

4.1. Interaction with a Non-degenerate Companion

Kasen (2010) presented simulations of an SN Ia interacting with a non-degenerate companion. This creates a shock cooling signature over the first few days, and has been a popular explanation for many of the early blue events (e.g., Marion et al. 2016; Hosseinzadeh et al. 2017). Other similar simulations predict a lower luminosity and shorter duration (Marietta et al. 2000; Maeda et al. 2014; Kutsuna & Shigeyama 2015), but are still potentially consistent with the early blue events depending on the size and distance of the companion.

If interaction with a non-degenerate companion produces early blue colors then one is left to explain why these objects have a preference to be 1991T/1999aa-like and of the Branch SS type. Moreover, the interaction model predicts the blue excess to be strongest when the companion sits between the explosion and the observer, so that less favorable viewing angles should still look red. Thus if this is the preferred explanation, then there should be early red events that are also bright and of the Branch SS type. However, such objects have yet to be discovered.

4.2. Presence of HV ^{56}Ni

Another way to produce additional heating at early times is if there is ^{56}Ni located in the very outer layers. This could be due to significant mixing by instabilities or large scale flows during the explosive burning. Alternatively, ^{56}Ni can be deposited in the outer layers from a helium-shell triggered double-detonation explosion (Woosley et al. 1980; Nomoto 1982), which can occur when there is a helium donor or even due to the helium-rich surface layers of a C/O WD during a double-degenerate merger. Such scenarios have been explored by Piro & Morozova (2016) and Magee et al. (2018), which find similar timescales, luminosities, and colors to the early blue events when there is $\sim$0.01 $M_\odot$ of ^{56}Ni in the surface layers.

The main criticism of the shallow ^{56}Ni explanation is whether a large abundance of iron group elements (IGEs) in the surface layers negatively impacts the spectra of SNe Ia at peak (Hoeflich & Khokhlov 1996; Nugent et al. 1997). More detailed treatments of the helium detonation (Shen & Moore 2014; Shen et al. 2018) and the converging shock in the C/O core (Shen & Bildsten 2014) find that this scenario may still be viable with smaller helium masses and less IGEs, but additional work is needed to understand whether it can both explain the early blue phase and still be consistent with the full spectral evolution of the events. Furthermore, the current set of observations and models do not have the fidelity to distinguish between a smooth, shallow mixed distribution of ^{56}Ni as focused on by Piro & Morozova (2016) and Magee et al. (2018) or a distinct blob of ^{56}Ni located near the surface as might be expected for a double detonation (see Maeda et al. 2018).

A related but slightly different way to produce additional early energy release is if there is nuclear burning in the outer layers (Hoeflich & Schaefer 2009). This differs from the double-detonation scenario in that a thin helium layer of $\sim 10^{-5} M_\odot$ mixed with some carbon (Wang et al. 2017) is triggered by the detonation front propagating out of the C/O core (rather than the helium layer igniting first). It has also been speculated that the helium layer could be triggered by g-modes driven by the convective simmering phase of carbon burning in single-degenerate scenarios (Piro 2011). In contrast, a hydrogen-rich layer would not burn due to the longer burning timescales which are well in excess of 1 s, compared to 10^{-2} s for a mixed helium–carbon layer.

4.3. Circumstellar Dust

Another potential source that could affect the early colors is varying amounts of circumstellar dust (Amanullah & Goobar 2011). However, this would require the dust to be fairly isotropic to avoid the unlikely proposition that the dust in the direction of the observer is always the same. Furthermore, the dust cannot impact the colors at peak which would require small patches of consistently well-aligned dust. While circumstellar dust may play a role in increasing the scatter in the color of early-time light curves, we do not believe it can create a correlation of early color with other observational properties as presented in this work.

4.4. Circumstellar Interaction

Yet another method for producing additional heat at early times is through the interaction of the ejecta with CSM. This could occur in the collision of the ejecta with distinct shells of material that are from the companion or pulsational events during the explosion itself. Taking a typical expansion velocity in the corresponding outer layers ($\sim$40,000 km s^{-1}) equates to a distance of $\sim 10^{15}$ cm (Hoeflich et al. 2002) within 3–5 days of $t_{\rm first}$. With this scale in mind, early emission could be produced from the conversion of kinetic energy of the ejecta into heating through its interaction with CSM (Gerardy et al. 2007; Dragulin & Hoeflich 2016; Noebauer et al. 2016). However, due to the short timescales covered by our early sample this is likely not a viable process as the CSM would have to be bound to the system of size less than $\sim 10^{15}$ cm, or in the direct vicinity.

Alternatively, the CSM could be more confined to the WD such as the tidally disrupted material that is present after a double-degenerate merger or the accretion flows in a single-degenerate scenario. In such cases, if the material is optically thick to the explosive shock wave, then the shock continues to propagate into the CSM and heat it (Piro & Morozova 2016). This produces a shock cooling signature at early times, with a luminosity that is proportional to the radius of the CSM. For the typical early luminosities of the early blue events, this implies a radius of $\sim 10^{11}$–10^{12} cm for such material. Further work is needed to better understand if the CSM would impact the spectra and light curve evolution in other ways that can be tested with observations.

4.5. Composition/Opacity Differences

A final possibility we consider is whether the early blue excess could actually not be due to additional energy input, but instead simply differences in opacity due to a different composition. If the outer layer of the ejecta is characterized by a lower opacity (e.g., due to a significant amount of unburnt carbon), the photosphere would recede more rapidly and thus reach the ^{56}Ni-rich region earlier. The overall affect of this is a faster release of energy, more heating, and thus bluer colors. This affect is demonstrated in Gall et al. (2018, see their Figure 11), where $10^{-2} M_{\odot}$ of unburnt carbon produces an earlier UV-blue phase lasting ≈4 days.

4.6. Closing Remarks

In conclusion, from the perspective of early phase colors, there appears to be at least two populations of SN Ia. Looking toward the future, the key question will be whether this represents a critical difference between the progenitors of these events, or if it is the result of smaller differences in composition, explosion energy, or some other detail of the explosions. Solving this mystery will require further theoretical modeling as well as gathering a larger sample of events to see how strongly this dichotomy persists and whether there are other properties that correlate with the early red and blue populations. While this manuscript was under review Jiang et al. (2018) presented an examination of early-excess SNe Ia. They also find a preference of blue, early-excess SNe Ia to be 1991T/1999aa-like. Their interpretation is consistent and complementary to our findings.

We thank P. Brown, G. Hosseinzadeh, J. Jiang, and A. Miller for promptly providing access to published data of several of the objects in our early sample. This work has been supported by a research grant 13261 (PI: Stritzinger) from the Villum FONDEN. M.D.S. is grateful to Aarhus University's Faculty of Science & Technology for a generous sabbatical grant. C.B., N.M., A.P., and M.P. acknowledge support from the National Science Foundation under grant AST1613426. E.B. and P.H. gratefully acknowledge support from NASA Grant NNX16AB25G. P.H. also acknowledge the NSF grants AST-1715133 and AST-1613472.

ORCID iDs

Maximilian D. Stritzinger https://orcid.org/0000-0002-5571-1833
Benjamin J. Shappee https://orcid.org/0000-0003-4631-1149
Anthony L. Piro https://orcid.org/0000-0001-6806-0673
E. Baron https://orcid.org/0000-0001-5393-1608
Peter Hoeflich https://orcid.org/0000-0002-4338-6586
Thomas W.-S. Holoien https://orcid.org/0000-0001-9206-3460
M. M. Phillips https://orcid.org/0000-0003-2734-0796
C. R. Burns https://orcid.org/0000-0003-4625-6629
Carlos Contreras https://orcid.org/0000-0001-6293-9062
Nidia Morrell https://orcid.org/0000-0003-2535-3091

References

Amanullah, R., & Goobar, A. 2011, ApJ, 735, 20
Benetti, S., Cappellaro, E., Mazzali, P. A., et al. 2005, ApJ, 623, 1011
Blondin, S., Matheson, T., Kirshner, R. P., et al. 2012, AJ, 143, 126
Bloom, J. S., Kasen, D., Shen, K. J., et al. 2012, ApJL, 744, L17
Branch, D., Dang, L. C., Hall, et al. 2006, PASP, 118, 560
Cartier, R., Sullivan, M., Firth, R. E., et al. 2017, MNRAS, 464, 4476
Childress, M. J., Scalzo, R. A., Sim, S. A., et al. 2013, ApJ, 770, 29
Contreras, C., Phillips, M. M., Burns, C. R., et al. 2018, ApJ, 859, 24
Dragulin, P., & Hoeflich, P. 2016, ApJ, 818, 26
Foley, R. J., Challis, P. J., Filippenko, A. V., et al. 2012, ApJ, 744, 38
Foley, R. J., Narayan, G., Challis, P. J., et al. 2010, ApJ, 708, 1748
Gall, C., Stritzinger, M., Ashall, C., et al. 2018, A&A, 611, 58
Gerardy, C. L., Meikle, W. P. S., Kotak, R., et al. 2007, ApJ, 661, 995
Goobar, A., Kromer, M., Siverd, R., et al. 2015, ApJ, 799, 106
Hoeflich, P., Gerardy, C. L., Fesen, R. A., & Sakai, S. 2002, ApJ, 568, 791
Hoeflich, P., & Khokhlov, A. 1996, ApJ, 457, 500
Hoeflich, P., & Schaefer, B. E. 2009, ApJ, 705, 483
Holmbo, S., Stritzinger, M. D., Shappee, B. J., et al. 2018, A&A Letters, submitted
Hosseinzadeh, G., Sand, D. J., Valenti, S., et al. 2017, ApJ, 845L, 11
Hsiao, E. Y., Burns, C. R., Contreras, C., et al. 2015, A&A, 578, A9
Im, M., Choi, C., Yoon, S.-C., et al. 2015, ApJS, 221, 22
Jiang, J.-A., Doi, M., Maeda, K., et al. 2017, Natur, 550, 80
Jiang, J.-A., Doi, M., Maeda, K., & Shigeyama, T. 2018, ApJ, in press (arXiv:1808.06343)
Kasen, D. 2010, ApJ, 708, 1025
Krisciunas, K., Contreras, C., Burns, C. R., et al. 2017, AJ, 154, 211
Kutsuna, M., & Shigeyama, T. 2015, PASJ, 67, 54
Li, W., Filippenko, A., Gates, E., et al. 2001, PASP, 113, 1178
Maeda, K., Jiang, J., Shigeyama, T., & Doi, M. 2018, ApJ, in press (arXiv:1805.12325)
Maeda, K., Kutsuna, M., & Shigeyama, T. 2014, ApJ, 794, 37
Magee, M. R., Sim, S. A., Kotak, R., & Kerzendorf, W. E. 2018, A&A, 614, 115
Marietta, E., Burrows, A., & Fryxell, B. 2000, ApJS, 128, 615
Marion, G. H., Brown, P. J., Vinkó, J., et al. 2016, ApJ, 820, 92
Marion, G. H., Vinkó, J., Wheeler, C. J., et al. 2013, ApJ, 777, 40
Miller, A. A., Cao, Y., Piro, A. L., et al. 2018, ApJ, 852, 100
Noebauer, U. M., Taubenberger, S., Blinnikov, S., et al. 2016, MNRAS, 463, 2972
Nomoto, K. 1982, ApJ, 257, 780
Nugent, P., Baron, E., Branch, D., Fisher, A., & Hauschildt, P. H. 1997, ApJ, 485, 812
Nugent, P., Phillips, M. M., Baron, E., Branch, D., & Hauschildt, P. 1995, ApJL, 455, 147
Nugent, P. E., Sullivan, M., Cenko, S., et al. 2011, Natur, 480, 344
Olling, R. P., Mushotzky, R., Shaya, E. J., et al. 2015, Natur, 521, 332
Pan, Y.-C., Foley, R. J., Kromer, M., et al. 2015, MNRAS, 452, 4307
Pereira, R., Thomas, R. C., Aldering, G., et al. 2013, A&A, 554, 27
Philips, M. M. 1993, ApJL, 413, 105
Piro, A. L. 2011, ApJL, 738, 5
Piro, A. L., Chang, P., & Weinberg, N. N. 2010, ApJ, 708, 598
Piro, A. L., & Morozova, V. S. 2016, ApJ, 826, 96
Piro, A. L., & Nakar, E. 2013, ApJ, 769, 67
Shappee, B. J., Piro, A. L., Holoien, T. W.-S., et al. 2016, ApJ, 826, 144
Shappee, B. J., Piro, A. L., Stanek, K. Z., et al. 2018, ApJ, 855, 6
Shen, K. J., & Bildsten, L. 2014, ApJ, 785, 61
Shen, K. J., Kasen, D., Miles, B. J., & Townsley, D. M. 2018, ApJ, 854, 52
Shen, K. J., & Moore, K. 2014, ApPhy, 797, 46
Silverman, J. M., Ganeshalingam, M., Cenko, S. B., et al. 2012, ApJ, 756L, 7
Stritzinger, M. D., Phillips, M. M., Boldt, L. N., et al. 2011, AJ, 142, 156
Vinkó, J., Sárneczky, K., Takáts, K., et al. 2012, A&A, 546, 12
Wang, B., Podsiadlowski, P., & Han, Z. 2017, MNRAS, 472, 1593
Wang, X., Filippenko, A. V., Ganeshalingam, M., et al. 2009, ApJ, 699L, 139
Woosley, S. E., Weaver, T. A., & Taam, R. E. 1980, in Proc. of Texas Workshop on Type I Supernovae (Austin, TX: Univ. Texas), 96
Yamanaka, M., Maeda, K., Kawabata, M., et al. 2012, ApJ, 782L, 35
Zhai, Q., Zhang, J.-J., Wang, X.-F., et al. 2016, AJ, 151, 125
Zheng, W. K., Shivvers, I., Filippenko, A. V., et al. 2014, ApJ, 783L, 24
Zheng, W. K., Silverman, J., Filippenko, A. V., et al. 2013, ApJ, 778L, 15